

Shallow Water Internal Waves and Associated Acoustic Intensity Fluctuations

P.V. Hareesh Kumar, K.V. Sanilkumar and V.N. Panchalai
Naval Physical and Oceanographic Laboratory, Kochi-682 021

ABSTRACT

Physical oceanographic and acoustic data were simultaneously collected from the coastal waters of the Arabian Sea. Acoustic transmissions were carried out from an anchored vessel using 620 Hz transducer and received by an array of hydrophones moored at ~5 km away from the anchorage. Thermal structure in this region was characterised by a tri-layer structure, ie, a strong thermocline (> 0.4 °C/m) sandwiched between an upper (< 10 m) and bottom (> 25 m) homogeneous layer. High-resolution (sampled at 10 s interval) temperature data from moored sensors revealed intense internal wave activity. The maximum value of Brunt-Vaisala frequency, which is the maximum frequency limit of internal waves in the thermocline, suggests that the upper frequency limit of the internal wave, which can be generated during this period, is 23 cph (2.6 min). High and low frequency waves caused variations of ~ 3 °C and ~ 5 °C respectively in the temperature field. But the low frequency internal waves were found to contain maximum energy compared to the high frequency waves. Fluctuations of 8-12 dB were noticed in the measured acoustic intensity values in the presence of low frequency internal waves. Simulation studies carried out using parabolic equation model using 620 Hz source indicated well-defined ducted propagation with minimum transmission loss, when the source was kept within the homogeneous layer. The presence of tri-layer thermal structure, ie, a strong gradient layer sandwiched between an upper and bottom homogeneous layer, caused surface and bottom channel propagation in this region.

Keywords: Tri-layer structure, internal waves, acoustic intensity fluctuations, acoustic propagation model

1. INTRODUCTION

Studies conducted over the past several years established internal waves as a dominant factor in causing fluctuations in the travel time of acoustic pulses sent over long distance through the ocean¹⁻³. The internal waves are considered to be a limiting factor in the propagation of acoustic energy in the frequency range 50 Hz to 20 kHz and the effects are manifested as amplitude and phase variations in the acoustic signal¹. These waves also limit the

temporal and spatial stability of acoustic paths. Long acoustic waves (< 50 Hz) are less likely affected by the internal waves.

Esser⁴, *et al.* carried out the first major experimental study to measure the total field acoustic fluctuations due to internal waves and also made efforts to model these fluctuations using model wave number perturbation approach. Zhou⁵, *et al.* conducted another experiment to study the scattering of acoustic energy by internal waves. They observed anomalous frequency

response in acoustic signal associated with shallow water internal wave and attributed this to the resonance between the acoustic mode coupling and the high frequency internal wavelength. Afterwards, Lynch⁶, *et al.* studied the acoustic travel-time fluctuations due to shallow water internal waves using a low-frequency transmitting source (224 Hz). Using the parabolic equation field calculations, Tang and Tappert⁷ showed the effects of internal waves on acoustic travel-time arrival. Konyaev⁸, *et al.* found that the presence of directional non-dispersive internal waves-caused acoustic fluctuations, which were highly coherent with time-lagged temperature. In another experiment, Rubestein⁹ also made an attempt to study the effect of Cnoidal internal on acoustic propagation in shallow waters. Rubenstein and Brill¹⁰ conducted a shallow water experiment using 400 Hz source and found that the transmission loss vary significantly over a wide range of time scales. They also observed the propagation of acoustic features across an array of hydrophone at 0.75-1 m/s, which is equal to the propagation speed of internal soliton waves. The time variation associated with this distortion results in fluctuation in acoustic intensity and phase in forward transmission experiment. The effect is of sufficient strength to constitute a major constraint in the design of acoustic transmission and detection systems. An acoustic experiment, SWARM, was conducted off the coast of New Jersey¹¹ to quantify the interaction of acoustic field

in the 10-1000 Hz band with linear and nonlinear internal waves in a shallow water waveguide. In spite of all these importance, the shallow water internal waves/acoustic interaction studies received less attention due to the complexities in the shallow waters.

In the coastal waters of India also, internal waves are found to be very prominent and cause large variability in the thermo-haline fields. However, specific acoustic experiments to assess the role of internal waves in causing acoustic intensity fluctuations are meagre. Hence, an experiment was conducted in the coastal waters of India to study the shallow water internal wave characteristics and their influence on acoustic propagation.

2. EXPERIMENTAL SETUP AND DATA

An acoustic buoy, attached with an array of five hydrophones at depths 8 m, 21 m, 36 m, 42 m and 47 m, was deployed in the shallow waters, where the bottom depth was 52 m (Fig. 1). The ship was then anchored at ~ 5 km away from the moored acoustic buoy. Acoustic signals transmitted using a 620 Hz projector, lowered to 15 m from the ship, served as the source. These signals were continuously transmitted for 2 min at every hour for 14 h (1200 h on 9 October to 0200 h on 10 October 2002) and received by the hydrophones. The received signals were stored on a tape recorder

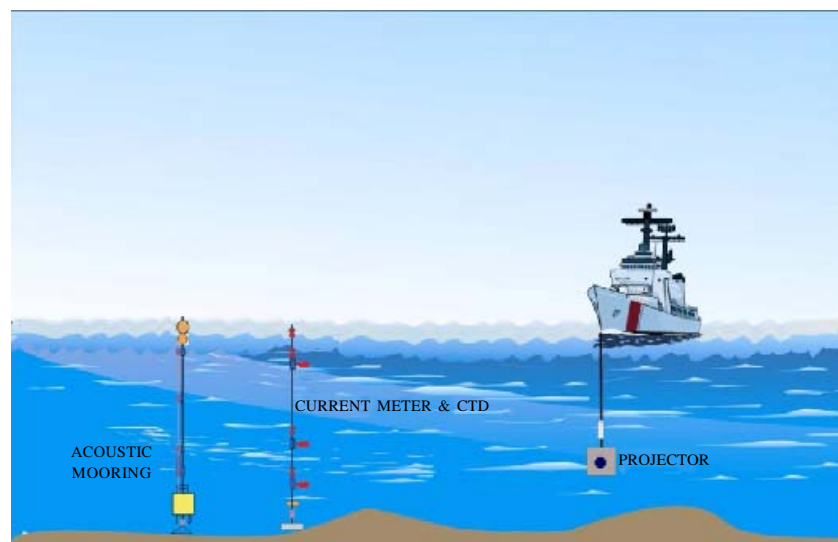


Figure 1. Experimental setup to study shallow water internal wave characteristic and their influence on acoustic propagation

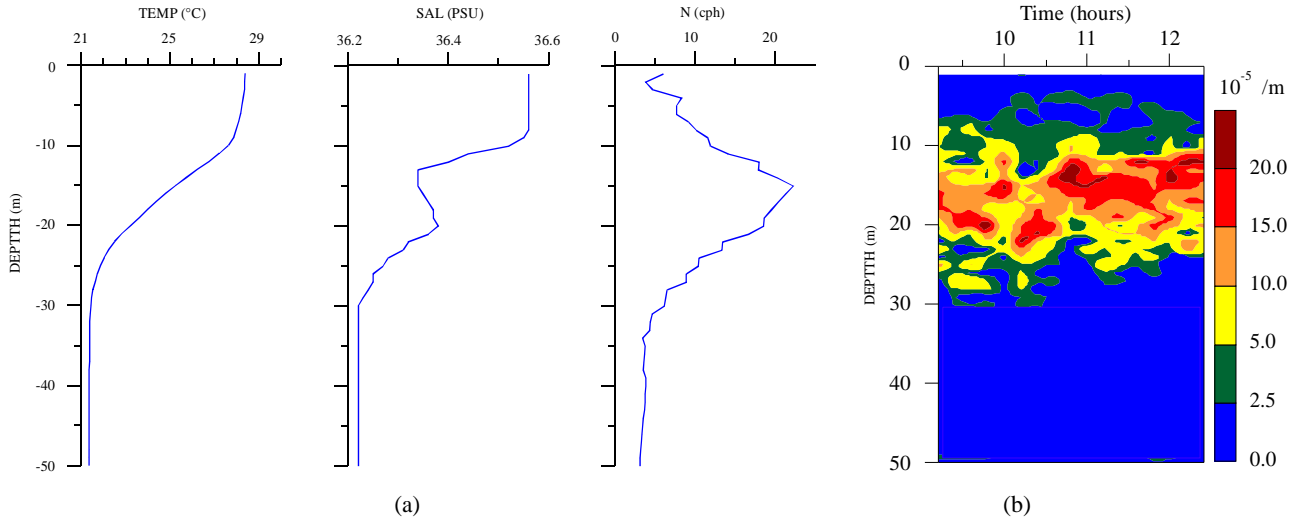


Figure 2. (a) Mean profiles of temperature, salinity, and Brunt-Vaisala frequency, N and (b) depth-time section of the stability parameter, E .

inside the acoustic buoy. To capture the temporal variability of internal waves and their impact on acoustic transmissions, three CTD's were attached in the hydrophone array (just above the hydrophones at 21 m, 36 m and 47 m depths). The sampling interval of data collection was chosen as 10 s to capture and delineate high frequency components of internal waves. Vertical profiles of temperature and salinity (using Mini CTD system) were collected from onboard the ship at 10 min interval for 3.5 h. Moreover, CTD casts were made along a transect of 20 km at every 5 km interval to get sound speed profiles required to understand the range-dependent characteristics of acoustic propagation in the vicinity of experimental site.

3. RESULTS AND DISCUSSION

The mean profiles of temperature, salinity, and Brunt-Vaisala frequency (N) at the time series station are presented in Fig. 2(a). The Brunt-Vaisala frequency is the upper frequency limit of the internal waves and is calculated from the vertical distribution of temperature and salinity using the relationship, $N^2(z) = -(g/\rho_0)(\delta\rho/\delta z)$. Here, g is acceleration due to gravity, ρ_0 is the average density, $\delta\rho/\delta z$ is the vertical density gradient, and z is the depth. To understand the temporal variability in the stratification characteristics, the depth-time section of the stability parameter, E is also presented [Fig. 2(b)].

In this region, the temperature profile is characterised by a thermocline of 15 m thickness (vertical gradient in excess of $0.44\text{ }^\circ\text{C/m}$, ie, $28\text{ }^\circ\text{C}$ at 10 m to $21.4\text{ }^\circ\text{C}$ at 25 m) sandwiched between upper (~ 10 m) and bottom homogeneous layers (~ 25 m). Similar feature is observed in the salinity structure also. This type of structure is known as tri-layer structure¹² and has significant influence on acoustic propagation (Fig. 5). The Brunt-Vaisala frequency indicated maximum values (23 cph) in the thermocline zone (~ 15 m) and minimum values in the surface and bottom isothermal layers. The stability parameter, E also indicated higher values between 10 m and 25 m, with maximum value ($>15 \times 10^{-5}/\text{m}$) around 15 m coinciding with the mid thermocline [Fig. 2(b)]. The stability parameter, E supports the occurrence of a strong thermocline in this region, which is one of the prerequisite conditions for the formation of internal waves. Moreover, the maximum value of N in the thermocline zone suggests that the upper frequency limit of the internal wave, which can be generated during this period, is 23 cph (2.6 min).

3.1 Internal Wave Characteristics

To have a detailed understanding of the internal wave characteristics, CTD's were attached (at 21 m, 36 m and 47 m depths) with the moored vertical hydrophone array for nearly 5 h (1 s interval) on 8th October 2002 and 14 h (10 s interval) during

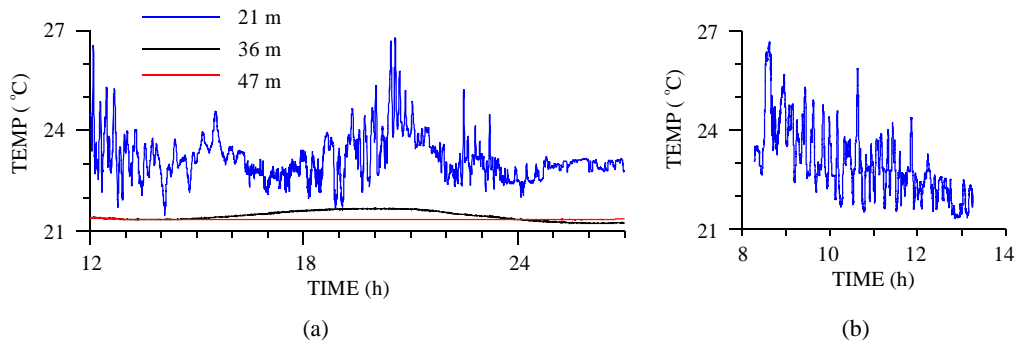


Figure 3. Time series of temperature variability at (a) 21 m, 36 m, and 47 m for 15 h during 9-10 October 2002 and (b) 21 m for 5 h on 8 October 2002.

9-10 October 2002. The sensor in the thermocline (ie at 21 m) showed the large fluctuations in the temperature field, both in the high frequency and low frequency domains [Figs. 3(a), 3(b)], indicating internal wave activity at this depth. For example, the temperature $< 22^{\circ}\text{C}$ noticed in the thermocline zone around 1800 h [Fig. 3(a)] increased to $\sim 27^{\circ}\text{C}$ by 2100 h, suggesting a variation of $\sim 5^{\circ}\text{C}$ over a period of 3 h. Even the data collected for a short duration, ie, nearly 5 h on 8th October [Fig. 3(b)] also indicated rhythmic oscillation in the temperature field. The temperature showed variation of more than 3°C within 30 min., ie, between 0830 and 0900 h [Fig. 3(b)]. These large amplitude fluctuations in the temperature field might have been due to the presence of highly stratified layer (Fig. 2). However, at 36 m and 47 m depth levels [Fig. 3(a)], such large amplitude temperature fluctuations were not seen, as the sensors were well within the bottom homogeneous layer.

To understand the major harmonics, the two data sets were subjected to FFT analysis and the results are presented in Fig. 4. The major harmonics noticed in the data sets collected during 9-10 October were in the bands of ~ 6 h (S1), ~ 3 h (S2) and ~ 3 to 6 min (S3). As the second data set was collected only for a short duration but with a higher sampling interval (1 s), the low-frequency components could not be resolved. Here also, the major harmonics observed in the high-frequency band (S3) coincided with the former case. It is to be noted that the low-frequency waves were found to contain maximum energy compared to the high-frequency waves. Even then, high-frequency internal waves were found to cause fluctuations of the order of $2\text{-}3^{\circ}\text{C}$ in the temperature field.

3.2 Theoretical Studies

Propagation models are the most common type of underwater acoustic models in use to understand

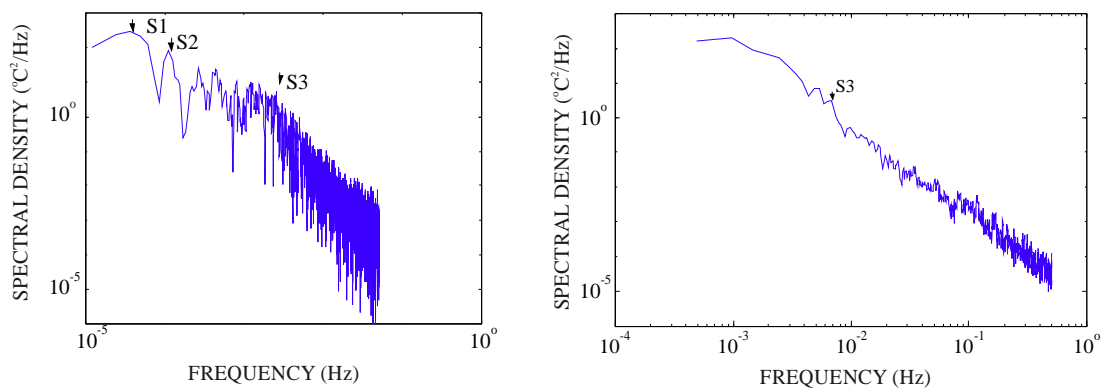


Figure 4. Spectral analysis of temperature data in the thermocline collected for (a) 15 h during 9-10 October 2002 and (b) 5 h on 8 October 2002. S1, S2, and S3 indicate peaks at ~ 6 h, ~ 3 h and near Brunt-vaisala frequency, ie, ~ 3 min, respectively.

the sonar performance problems¹³. Various acoustic propagation models are available in the literature based on the theoretical approach employed. In one approach, range-dependent case has been considered, in which the properties of the ocean medium vary as a function of range and azimuth from the receiver, in addition to depth dependence. This type of model includes sound speed profiles and bathymetry at discrete spatial intervals.

The basic wave equation is

$$\nabla^2 \phi = \frac{1}{C^2} \frac{\partial^2 \phi}{\partial t^2} \quad (1)$$

where, ∇ is the Laplacian operator, ϕ is the potential function, C is the speed of sound, and t is the time. After incorporating harmonic solution to obtain the time-dependent Helmholtz equation, the Eqn (1) reduces to

$$\nabla^2 \phi + k^2 \phi = 0 \quad (2)$$

Here $k = \omega/c = 2\pi/\lambda$ is the wave number, ω is source frequency, and λ is the wavelength.

The parabolic approximation approach replaces the elliptic wave equation with a parabolic equation (PE). The PE is derived by assuming that energy propagates at speed—either the shear speed or compressional speed, as appropriate.

Then the basic equation of acoustic propagation can be written as

$$\nabla^2 \phi + k_0^2 n^2 \phi = 0 \quad (3)$$

Here n is the refractive index.

The Eqn (3) can be rewritten in cylindrical coordinates as

$$\frac{\partial^2 \phi}{\partial r^2} + \frac{1}{r} \frac{\partial \phi}{\partial r} + \frac{\partial^2 \phi}{\partial z^2} + k_0^2 n^2 \phi = 0 \quad (4)$$

where the azimuthal coupling has been neglected but the index of refraction retains a dependence

on azimuth. Further, assume a solution of the form $\phi = \psi(r,z)S(\theta)$ and obtain an equation in ψ and another equation in S . The equation in S has the solution given by Hankel function of first kind. The equation in ψ , after applying the far-field and paraxial approximation, can be written as

$$\frac{\partial^2 \psi}{\partial z^2} + 2ik_0 \frac{\partial \psi}{\partial r} + k_0^2 (n^2 - 1) \psi = 0 \quad (5)$$

which is the parabolic wave equation. In this equation, n depends on depth (z), range (r) and azimuth (θ). This equation can be numerically solved by implicit finite difference (IFD) method.

In the PE approximation, the Helmholtz equation is converted to a parabolic equation with only first derivatives in the range variable. This allows efficient numerical solution by non-iterative marching techniques. The size of the range steps in the marching allows for inclusion of range-dependent interfaces comprising the ocean bottom and sub-bottom structure as well as range-varying oceanic features such as internal waves, fronts, eddies, thermohaline structure, etc. These two major capabilities, viz., efficient numerical solutions on small computers and the ability to model complex ocean environmental features have made the ocean acoustic PE models the most popular choice of both research and operational modelers^{14,15}.

The analysis indicated that the vertical thermal structure in this region is characterised by the presence of a tri-layer structure. To understand the range-dependent transmission loss (TL) in the presence of this type of tri-layer structures, the acoustic propagation model¹⁶ based on parabolic equation method was used. The model was run for a low-frequency source (620 Hz) in the down-slope scenario by keeping the source at the surface homogeneous layer (8 m), thermocline (20 m) and bottom homogeneous layer (35 m).

When the source was within the surface homogeneous layer [Fig. 5(a)], propagation in the surface layer, ie, ducted propagation with minimum transmission loss (TL < 100 dB) was well pronounced compared to other two cases [Figs 5(b) and 5(c)].

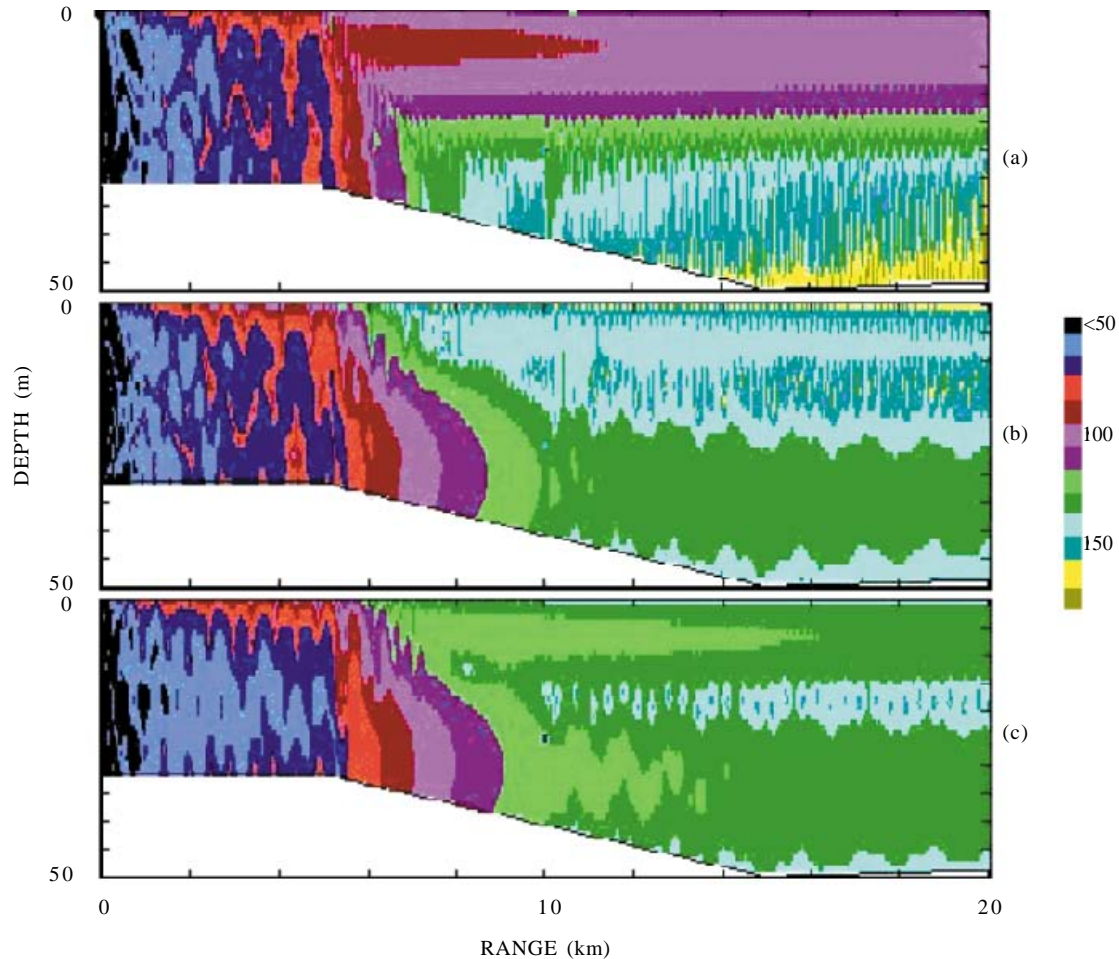


Figure 5. TL mosaic (in dB) of the model by keeping source (620 Hz) in: (a) surface homogeneous layer, 8 m, (b) thermocline, 20 m, and (c) bottom homogeneous layer, 35 m.

In this case, the 100 dB TL mosaics extended to more than 20 km. But, when the source location was shifted to the mid thermocline [Fig. 5(b)], TL in the surface layer increased. But, a well-defined bottom channel became evident. In this situation, the 100 dB TL mosaic extended only up to 6 km in the surface channel, but it was noticed up to 8 km in the bottom channel. In the third case, ie, when the source was kept in the bottom homogeneous layer, TL decreased in the surface and bottom channels [Fig. 5(c)] compared to the second case [Fig. 5(b)]. In this case, the surface and bottom channel propagation became well-marked.

This study highlights the fact that well-ducted propagation with minimum TL occurs when the source was within the homogeneous layer. Moreover, the two-channel propagation was possible because

of the presence of a strong gradient layer sandwiched between surface and bottom homogeneous layers.

3.3 Acoustic Intensity Fluctuations

The analysis of temperature in the thermocline revealed the dominance of both low (~6 h) and high frequency (~3 min) internal waves in this region. To study the influence of these internal waves, acoustic signals transmitted using a 620 Hz transducer lowered to 15 m depth (thermocline) and received by a hydrophone array moored at a distance of 5 km away were utilised. The received acoustic signals were very weak at 8 m and 21 m, and hence, not included for discussion. The TL mosaics [Fig. 5(b)] also indicated increase in the transmission loss in the surface homogeneous layer, ie, reduction in the acoustic energy, when the source

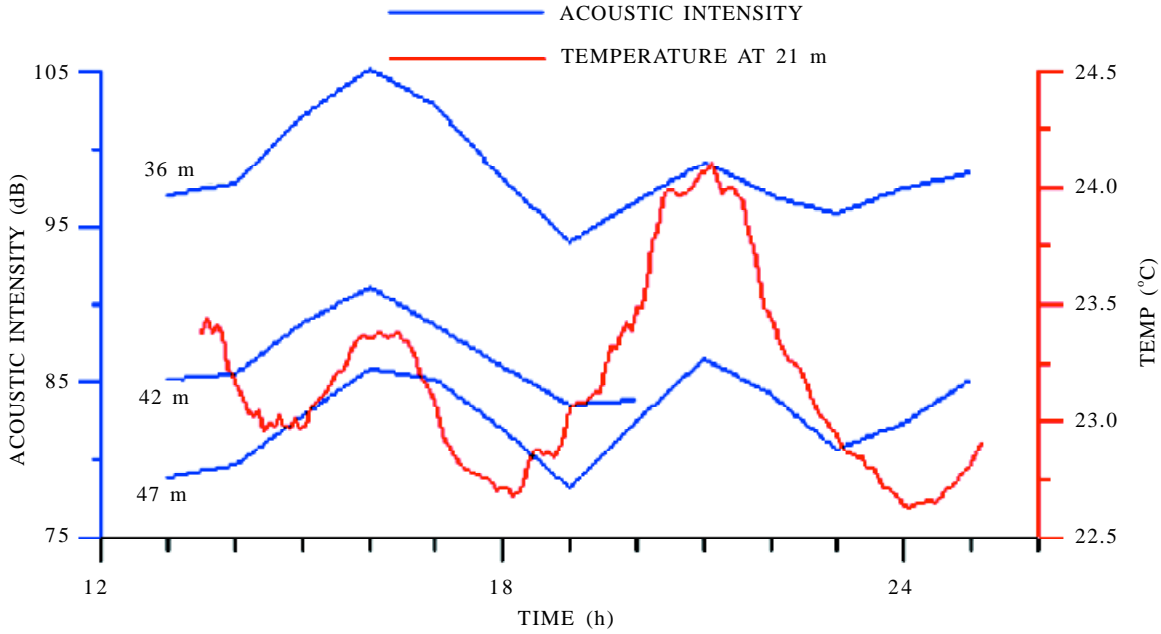


Figure 6. Hourly time series of acoustic intensity fluctuation (blue line) and temperature in the thermocline (red line)

was kept in the thermocline. For the other levels (36 m, 42 m, 47 m), the signals were stronger, and therefore, the intensity values at these levels could be retrieved. The measured acoustic intensity values

were averaged for each transmission (ie, for 2 min durations) and presented along with the hourly averaged temperature in the thermocline (Fig. 6).

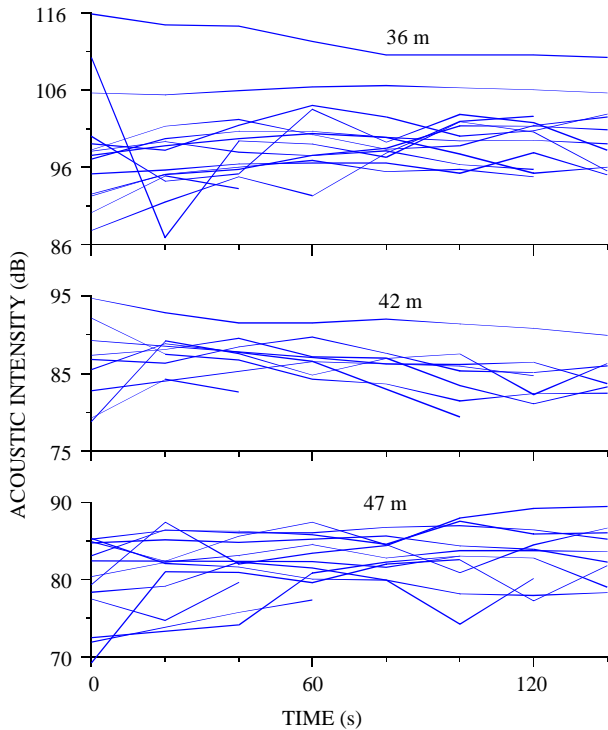


Figure 7. Composite plots of acoustic intensity for the entire 14 transmissions each of 2 min durations at every hour.

The temperature record indicated internal waves with 6 h periodicity with peaks at 1600 h and 2200 h, which was also revealed by the FFT analysis (Fig. 4). The disjoint nature of the acoustic transmission (hourly transmission each for 2 min. duration) prevented from making strong correlation between the acoustic intensity variability and internal wave fields. Even then, it is to be noted that this low frequency internal wave (6 h periodicity) caused a variation of ~8 to 12 dB in the acoustic intensity values, with maximum intensity values at the trough and minimum at the crest of the wave. This may be due to the increase/decrease in the sonic layer thickness associated with the arrival of trough/crest of the internal wave.

To understand the high frequency variability of the acoustic signals, the hourly intensity values recorded for 2 min durations were averaged for every 20 sec and presented as composite plot for the entire 14 transmissions (Fig. 7). The notable observations from this figure is the large spread (>10 dB) in the acoustic intensity values at all levels over a period of 14 h. The maximum spread (>15 dB) was noticed just below the thermocline,

ie, at 36 m. As the signals were transmitted at hourly time intervals, the large variability in the acoustic signals may be caused by the passage of low frequency internal waves, as revealed by the FFT analysis (Fig. 4).

This analysis clearly brought out the importance of internal wave activity both in the low frequency and high frequency domains. The low frequency internal waves caused a fluctuation of 8-12 dB in the acoustic intensity values. Moreover, the tri-layer structure was found to favour surface and bottom channel propagation. In the presence of this type of thermal structure, minimum TL and maximum range was found to occur when the source was kept in the surface homogeneous layer.

ACKNOWLEDGEMENTS

Authors are thankful to the Director, Group Head, and Head of Physical Oceanography Division for their constant encouragement, interest and support provided during the course of this work.

REFERENCES

1. Flatte, S.M.; Dishen, R.; Munk, W.H.; Watson, K.M. & Zachariasen, F. (Eds). Sound propagation through a fluctuating ocean. Cambridge University Press, Cambridge, UK, 1979. 44-61.
2. Duda, T.; Flatte, S.M.; Colosi, J.; Cornuelle, B.; Hildebrand, J.; Hodgkiss, W.; Worcester, P.; Howe, B; Mercer, J; & Spindel, R. Measured wave front fluctuations in 1000 km pulse propagation in the Pacific Ocean. *J. Acous. Soc. Am.*, 1992, **92**, 939-55.
3. Colosi, J.; Flatte, S.M. & Bracher, C. Internal wave effects on 1000 km oceanic acoustic pulse propagation: Simulation and comparison with experiment. *J. Acous. Soc. Am.*, 1994, **96**, 452-68.
4. Essen, H.H.; Schirmer, F. & Sirkes, S. Acoustic remote sensing of internal waves in the shallow water. *Int. J. Remote Sens.*, 1983, **4**, 33-47.
5. Zhou, J.X.; Chang, X.Z. & Rogers, P.H. Resonant interaction of sound wave with internal solitons in the coastal zone. *J. Acous. Soc. Am.*, 1991, **90**, 2042-054.
6. Lynch, J.F.; Jin, G.; Pawlowics, R.; Ray, D.; Chiu, C.S.; Miller, J.H.; Bourke, R.H.; Parsons, A.R.; Plueddemann, A.J. & Muench, D. Acoustic travel-time fluctuation due to shallow water internal waves in the Barents Sea Polar Front: Theory and experiment. *J. Acous. Soc. Am.*, 1996, **99**, 803-21.
7. Tang, X. & Tapper, F.D. Effects of internal waves on sound pulse propagation in the straits of Florida. *IEEE J. Oceanic Engg.*, 1997, **33**, 245-55.
8. Konyaev, K.V.; Sabinin, K.D.; Tuzhikin, Y.I. & D'yatchenko, V.R. Signal changes on stationary acoustical track under action of internal waves. Proceedings of the 8th International Symposium on Acoustic Remote Sensing and Associated Techniques of the Atmosphere and Ocean, Moscow, ISARS'96. 1996. pp. 235-40.
9. Rubenstein, D. Observations of Cnoidal internal waves and their effect on acoustic propagation in shallow waters. *IEEE J. Oceanic Engg.*, 1999, **24**, 346-57.
10. Rubenstein, D. & Brill, M.H. Acoustic variability due to internal waves and surface waves in shallow water. *In* Ocean Variability and acoustic propagation, edited by J. Potter and W. Warn-Varnas, Kluwer Academic Publishers, London, 1990. pp. 215-28.
11. Apel, J.R.; Badiay, M.; Chiu, C.; Finette, S.; Headrick, R.; Kemp, J.; Lynch, J.F.; Newhall, A.; Orr, M.H.; Pasewark, B.H.; Tielbuerger, D.; Turgut, A.; Von der Heydt, K. & Wolf, S. An overview of the 1995 SWARM shallow water internal wave acoustic scattering experiment. *IEEE J. Oceanic Engg.*, 1997, **22**, 465-500.
12. Hareesh Kumar, P.V.; Pradeep Kumar, T.; Sunil, T. & Gopakumar, M. Observations on the relationship between scattering layer and mixed layer. *Current Science*, 2005, **88**, 1799-802.
13. Etter, P.C. Underwater acoustic modelling. 1996, E& FN SPON, London.

14. Collins, M.D. Higher-order Pade approximations for accurate and stable elastic parabolic equations with application to interface wave propagation. *J. Acoust. Soc. Am.*, 1991, **89**. 1050-057.
15. Davis, J.A.; White, D. & Cavanagh, R.C. NORDA Parabolic Equation Workshop, 31 March-3 April 1981, Naval Ocean Research Development Activity, 1982. Tech. Note No. 143.
16. Balasubramanian. P.; Radhakrishnan, K.G. & Muni, M.M. PRAN (Sonar Range Predication Model Ver 1.0), NPOL, Kochi, India. 1997. NPOL-RR-6/97

Contributors



Dr P.V. Hareesh Kumar is working as Scientist F at Naval Physical and Oceanographic Laboratory (NPOL), Kochi. He obtained his MSc (Oceanography) and PhD (Oceanography) from Cochin University of Science and Technology (CUSAT). His field of specialization include: Air-sea interaction, mixed layer dynamics, Thermohaline structure, ocean modelling, sonar oceanography, etc. He has published 39 papers in national/international journals. He is a life member of Indian Meteorological Society, Indian Society of Remote Sensing, and Administrative Staff College of India Association, Hyderabad.



Dr K.V. Sanilkumar is working as Scientist E at NPOL, Kochi. He obtained his MSc (Oceanography) and PhD (Oceanography) from CUSAT. He was given *Dr BN Desai Award* (1995-96). He has published 20 papers in research journals. He is a life member of Indian Meteorological Society, and Indian Society of Remote Sensing.



Shri V.N. Panchalai obtained BE (Electrical and Electronics Engg) from the Regional Engineering College, Tiruchirappalli, Bharadhidasan University. His areas of specialisation include: Underwater acoustic experiments, data acquisition and data analysis. He is associate member of Institution of Engineers.